Journal of Power Sources, 2 (1977/78) 241 - 256

EVALUATION OF CYCLIC VOLTAMMETRY FOR ACCELERATED CORROSION LIFE TESTS OF THE PbO_2 ELECTRODE

J. L. WEININGER

Research and Development Center, General Electric Company, Schenectady, N.Y. 12301 (U.S.A.)

(Received March 7, 1977; in revised form July 27, 1977)

Summary

Cyclic voltammetry, electrochemical measurements at constant potential, and metallography were used to follow the anodic activity of chill-cast and wrought pure Pb and ternary Pb–Ca–Sn alloys as well as cast and wrought Pb–Sb. Cyclic voltammetry showed the formation of irreversible PbO_2 during a 1000 cycle test and also brought to light a diffusion or barrier-limited process during the cathodic discharge of calcium-containing alloys. Constant potential measurements could be correlated with corrosion behavior. The relative anodic activity was ranked for all samples tested. In general, chill-cast material showed less anodic activity than wrought materials, and ternary alloys less than pure lead, although in some cases the difference was very small.

Zusammenfassung

Die anodische Aktivität von kalt geformten und bearbeiteten reinem Blei und ternärer Blei–Kalzium–Zinn Verbindung wurde mit Hilfe von zyklischer Voltammetrie, elektrochemischen Messungen bei konstantem Potential, und Metallograph untersucht. Die zyklische Voltammetrie zeigte eine irreversibel Formation von PbO_2 während 1000 Zyklen. Ein Vorgang, der von Diffusion oder einem anderen Zeit-beschränkten Vorgang herrührt, wurde für kathodische Entladung der Kalzium-enthaltenden Verbindungen festgestellt. Die relative anodische Aktivität von allen Proben zeigte, dass kalt-geformte Materialen im allgemeinen weniger korrodierten als bearbeitete Metalle, und ternäre Verbindungen weniger als reines Blei. In manchen Fällen war aber dieser Unterschied klein.

Introduction

Cyclic and linear sweep voltammetry (hereafter denoted by CV and LSV) have been used extensively to elucidate partial and complete electrode

reactions. They have also been applied with considerable success to the electrodes constituting the lead–acid cell [1 - 4]. Experimental conditions, such as sweep rate and the chosen potential limits, determine the often complex form of the current–voltage relation. Oxides, sulfates, and their combined products, can be formed in the potential range between the very negative reduced metallic lead (with possible hydrogen evolution), and the very positive PbO_2 electrode (with possible concurrent oxygen evolution). In addition to the formation of these compounds, kinetic effects due to different reaction sites, surface morphology, and crystal structure, as well as non-Faradaic effects, may all be reflected in the shape of the voltammogram. A simplification results by limiting the potential range of LSV or CV to a region of particular interest to battery technology. In the present work CV was restricted to the range in which the positive plate of the lead–acid battery operates during cycling. Emphasis on the oxidation behavior of lead and some of its alloys was to provide an empirical accelerated life test of the corroding grids.

Methods

Figure 1 illustrates the method. The current–voltage trace is one of a series of cyclic triangular voltage sweeps, comparing the anodic capacity, during that sweep, with the cathodic capacity. The anodic and cathodic peaks are particularly sharp because of the very slow sweep rate of 0.1 mV/s. The cycle starts at about the theoretical value of the potential corresponding to the reaction:

$$PbSO_4 + 2H_2O = PbO_2 + H_2SO_4 + 2H^+ + 2e^-$$

E° = 1.196 V *vs.* Hg/Hg_2SO_4 in 1.28 s.g. H_2SO_4
(1.684 V *vs.* H_2/H^+ in same solution)

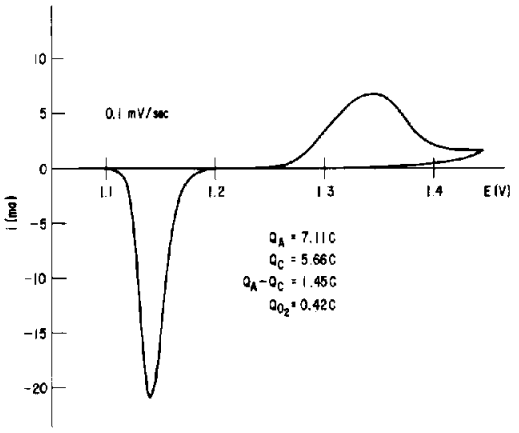

Fig. 1. Voltammogram of pure Pb electrode, surface area 4 cm^2; sweep rate 0.1 mV/s.

As this reaction goes to completion and oxygen begins to evolve, the sweep is reversed. The cathodic reduction has a more pronounced current peak, showing that the reduction, simulating the discharge of the battery is less hindered than the anodic oxidation (battery charge).

Several steps, other than the charge transfer in the overall reaction above, may occur at the positive electrode of the lead–acid cell. There are limiting diffusion and recrystallization steps in the reactions which modify the CV traces [5 - 7]. These are dependent on the CV conditions, for example, the potential range and sweep rate of the CV, as well as the previous history of the test electrode. In the present CV work the experimental conditions gave a minimum of kinetic steps which could interfere with the cycling between the oxidized (charged) β-PbO_2 and the reduced (discharged) $PbSO_4$ active material. On Fig. 1, Q_a is the anodic charge, which on potential reversal leads to Q_c, the cathodic charge. Their net difference, $Q_a - Q_c$, is the coulombic charge per cycle which goes into an irreversible oxidation of the substrate. It represents the charge associated with ongoing corrosion plus a relatively small amount of oxygen evolution.

At faster sweep rates, the peaks are less clearly defined. Consequently, a rate of 5 mV/s was chosen as the fastest feasible rate without losing the essential details of the cathodic portion of the voltammogram (Fig. 2).

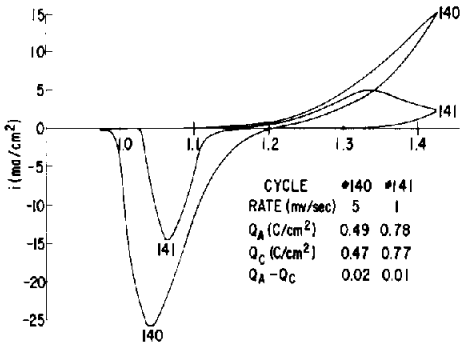

Fig. 2. Voltammograms of wrought pure Pb electrode at 1 and 5 mV/s; cycles 140 and 141.

Thus, it was possible to monitor 1000 cycles in 50 h, accelerating greatly a process that simulated the charge–discharge cycling of a battery grid.

The following parameters, pertinent to the corrosion process, were measured: (I) $Q_a - Q_c$ when plotted against cycle life, gives a linear relation, the slope of which represents the current density, or that part of the CV current going into irreversible build-up of oxidation product. Known current densities for oxygen evolution on β-PbO_2 at the given potentials [8] indi-

Fig. 3. Chill-cast pure Pb; 100×. Note irregular subgrains consisting of convection cells.

cate that oxygen evolution can be the source of only a small fraction of the quantity $Q_a - Q_c$. (II) The cumulative effect of a 1000 cycle test is represented by the final value of $Q_a - Q_c$ at 1000 cycles. This charge, divided by the total time of the experiment, again may represent a corrosion current density. (III) The magnitude of Q_c represents the reducible part of the oxidation product over the cycle life, and hence may reflect the extent of corrosion during cycle life.

In addition, constant potential measurements were performed at 1.300 and 1.400 V *vs.* Hg/Hg_2SO_4 for periods of 24 hours. Although not as representative of grid corrosion as previous constant potential measurements [9], which extended over a period of 5000 hours, these tests were intended for comparison of constant potential and CV measurements and further for empirical ranking of corrosion resistance of the various grid alloys.

Experimental

Metallography

The CV method described above was used for corrosion tests on the following samples of lead and lead alloys: (1) chill-cast pure lead (Cominco);

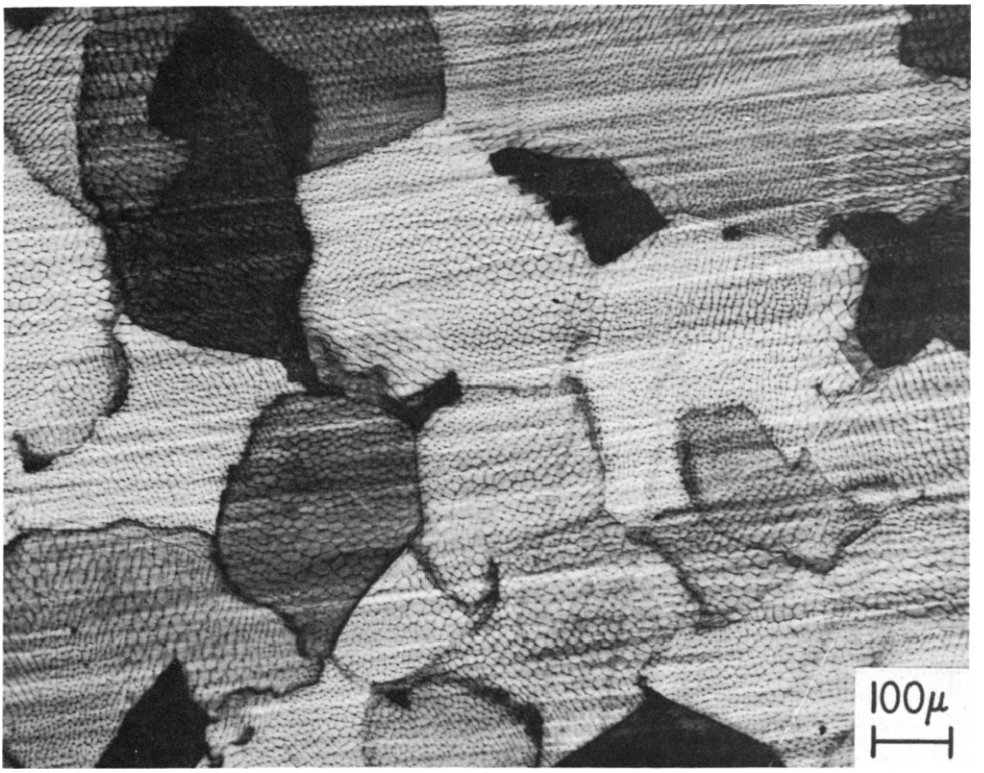

Fig. 4. Chill-cast ternary alloy Pb–0.053 Ca–0.70 Sn; 100×. Regular hexagonal subgrains viewed in direction of solidification.

(2) chill-cast ternary alloy Pb/0.05 Ca/0.70 Sn (Cominco); (3) cast binary alloy Pb/5.7 Sb (Cominco); (4) wrought pure lead (St. Joe Minerals Corp.); (5) wrought ternary alloy Pb/0.07 Ca/0.70 Sn (St. Joe Minerals Corp.)

All of these samples were examined by metallography because corrosion is dependent on grain structure.

The chill-cast samples had very large grain sizes, with a cellular structure within the grains. This structure is somewhat irregular in the case of chill-cast pure lead (Fig. 3); it is very regular and hexagonal in the ternary chill-cast alloy when viewed from the top (Fig. 4) and columnar when viewed at right angles, *i.e.* normal to the direction of cooling (Fig. 5). Such a side view of a lead casting was recently described by Caldwell and Sokolov [10].

The Pb/5.7 Sb alloy (Fig. 6) showed many free dendrites in a structure typical of the antimonial lead used in lead–acid batteries.

The wrought pure lead (sample 4) showed large grains, with an average grain size of about 100 μm, typical of a cast sheet (Fig. 7). No grain refinement, possibly resulting from the reduction of thickness from 0.75 to 0.35 in., could be noted. Such grain refinement was clearly seen in the wrought ternary Pb/0.07 Ca/0.70 Sn alloy of sample 5 (Fig. 8).

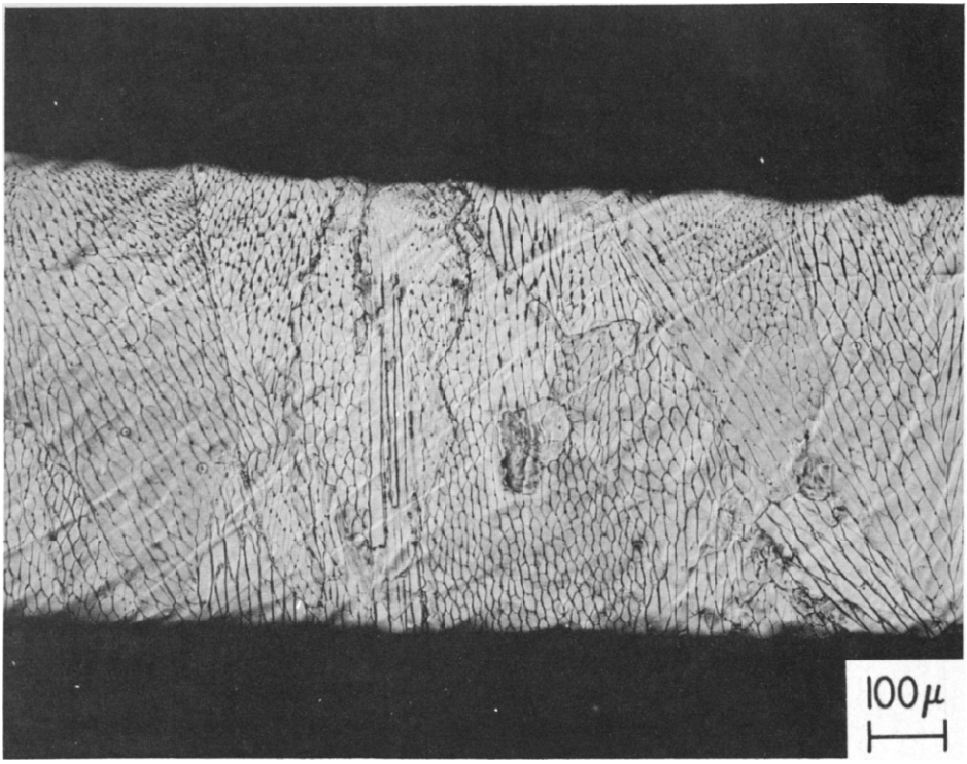

Fig. 5. Chill-cast ternary alloy; 100X. Sample of Fig. 4 viewed perpendicularly to the direction of solidification.

Procedure

Rectangular test samples, 4 cm long, with approximately 4 cm^2 total surface area, were located within a cylindrical electrolyte volume, defined by a large pure lead counter electrode. The solution was provided with H_2/H^+ and Hg/Hg_2SO_4 reference electrodes. An inert gas stream produced mild stirring and prevented atmospheric oxygen from participating in the electrode reactions.

The samples were degreased and atmospheric oxidation products were removed by immersion in a solution at 50 °C containing 10% by wt. of NaOH, 2% mannitol and 1% $N_2H_4 2HCl$ in distilled water. A brief chemical polish with an aqueous solution containing 20% (by vol.) CH_3COOH + 10% H_2O_2 (30%) at room temperature followed for all electrodes except the Pb/Sb alloy which was non-uniformly attacked by the acid polish.

After drying and weighing, the electrodes were immersed in the 1.28 s.g. H_2SO_4 test solution, saturated with $PbSO_4$, where they quickly reached the theoretical $Pb/PbSO_4$ potential of −0.954 V. They were then polarized mildly at +1.000 V to oxidize the samples superficially to the extent of about 0.05 C/cm^2. Cycling was then started at 5 mV/s in the potential range +0.975 to +1.425 V *vs.* Hg/Hg_2SO_4. The upper limit of this range corres-

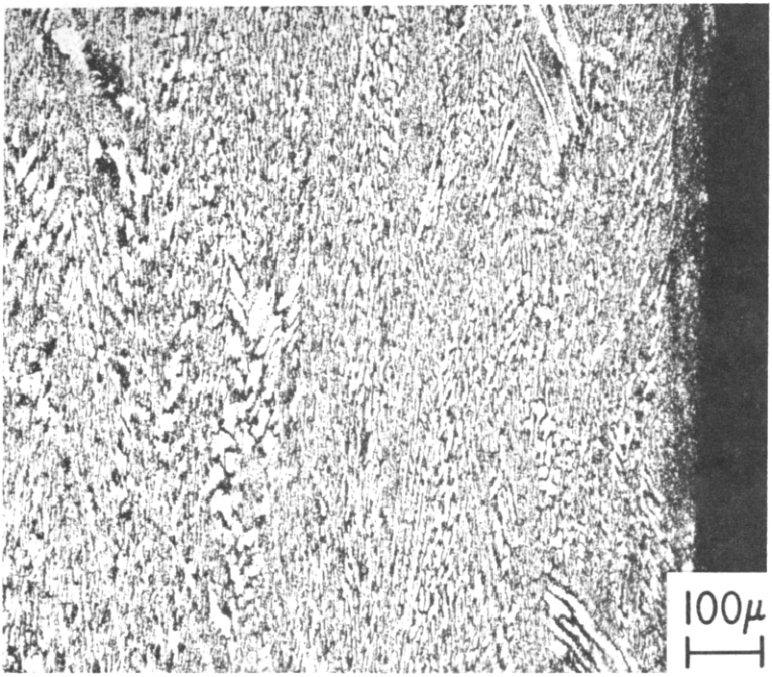

Fig. 6. Cast and rolled Pb–5.7 Sb alloy; 100×.

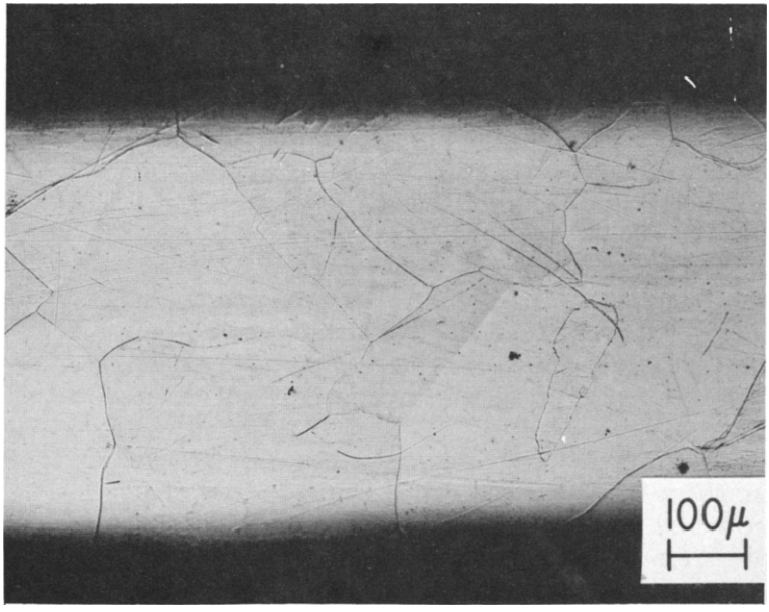

Fig. 7. Cast and rolled pure Pb; 100×, note large grain size, lack of grain refinement.

ponded to anodization to the maximum potential which a PbO_2 electrode would experience during cycling without undue evolution of oxygen. The

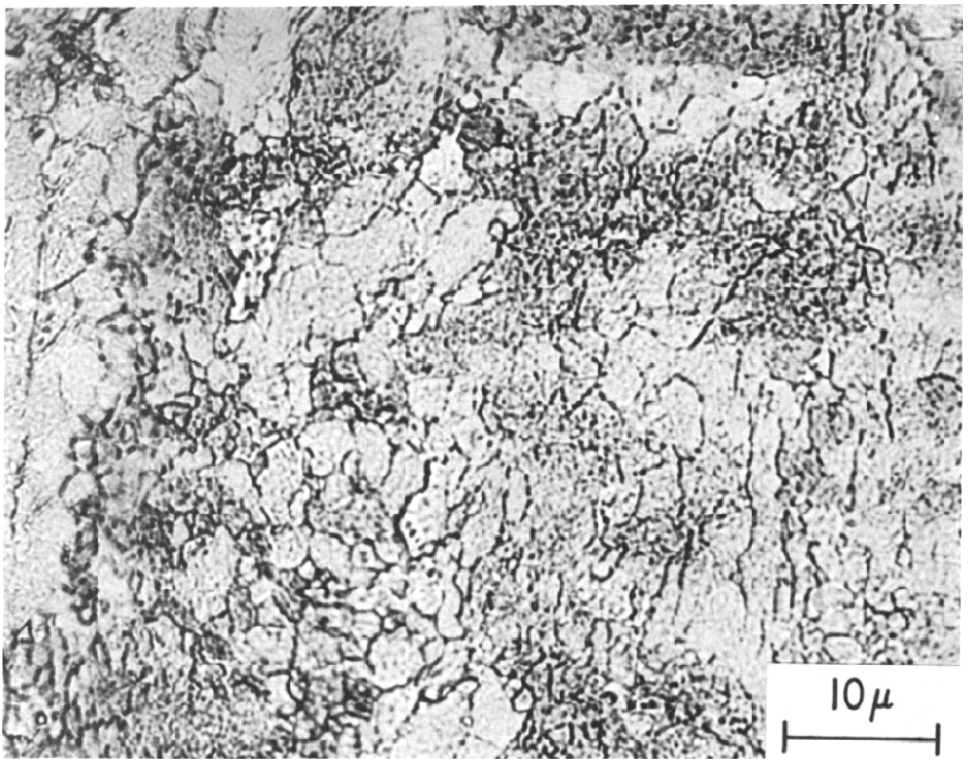

Fig. 8. Wrought ternary alloy Pb–0.07 Ca–0.70 Sn, 2000×, note grain-refined fine structure.

lower limit corresponded to the complete reduction of accessible PbO_2 in each cycle. The above range and rate were adhered to continuously for the duration of 1000 cycles, except that the rate was changed to 1 mV/s two or three times in the course of the test in order to monitor and establish better definition of the cyclic voltammogram. For example, Fig. 2 shows successive cycles No. 140 and 141, at the two different sweep rates on a wrought pure lead electrode. During the cycling a digital coulometer (Princeton Applied Research Inc.) cumulatively recorded the charges passing through the cell. For individual cycles, Q_c and $Q_a - Q_c$ were obtained directly from the coulometer.

At the end of an experiment, the electrodes were washed with distilled water, dried overnight in vacuum and weighed. Subsequently, the corrosion product was removed by the alkaline solution with the procedure mentioned above. The samples were again washed, dried and weighed in order to obtain the weight of the corrosion product.

For constant potential experiments at 1.300 and 1.400 V for 24 hours, the electrodes were prepared in the same manner as for CV experiments. Again, the coulometer was used to follow the charging except that in this procedure, only anodic charging took place.

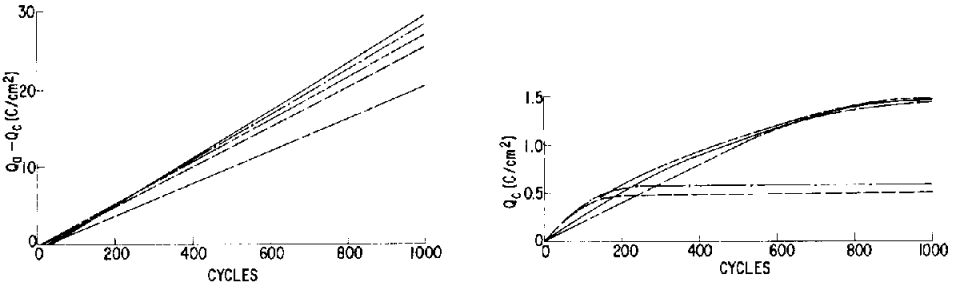

Fig. 9. Cumulative net anodic activity during cycle life. ———, chill-cast pure Pb; — — — —, chill-cast ternary alloy; —— — —— —, cast Pb/Sb; —— — — —— —, wrought pure Pb; — · — · —, wrought ternary alloy.

Fig. 10. Cathodic charge per cycle *versus* cycle life. ———, chill-cast pure Pb; — — —, chill-cast ternary alloy; —— — —— —, cast Pb–Sb; —— — — —— —, wrought pure Pb; — · — · —, wrought ternary alloy.

Results

Cyclic voltammetry

Two of the main features of the voltammograms, such as those shown in Figs. 1 and 2, are the coulometric determinations as a function of cyclic life of: (i) the net excess anodic charge, $Q_a - Q_c$ and (ii) the cathodic charge, Q_c, only. These relations are presented graphically in Figs. 9 and 10 for the five different lead and lead alloys which were studied.

Figure 9 represents least-square-fits of $\Sigma(Q_a - Q_c)$ from two to four experiments on each material. The slopes of the curves in Fig. 9 give an average anodic net current density. Similarly, the final value of $\Sigma(Q_a - Q_c)$, when averaged over the duration of 1000 cycles, is a measure of average net current density. These current densities are listed in Table 1, arranged in order of decreasing values.

Figure 10 shows the change in Q_c, per cycle, as a function of cycle life. Both ternary alloys, wrought Pb–0.07 Ca–0.7 Sn and chill-cast Pb–0.053 Ca–0.7 Sn, have Q_c levelling off at a plateau value at about 200 cycles. Current densities are difficult to assign because the plots are not linear. The pure Pb samples, independent of their method of preparations at first increase linearly, then monotonically at a diminishing rate to a final value of Q_c at 1000 cycles that corresponds to an average cathodic current density of about 30 mA/cm^2.*

Weight determinations

Average weight gains resulting from the 1000 cycle life-test were determined for each electrode material: 2.3, 2.7, 3.4, 5.3, and 6.1 mg/cm^2,

*A value of 1.5 C/cm^2 for Q_c, measured over a potential range of 250 mV/cycle at 5 mV/s gives 1.5 × 1000 × (5/250) = 30 mA/cm^2.

TABLE 1

Net average anodic current density during cycle tests

Sample No.	Material	Based on slope of $(Q_a - Q_c)$ *vs.* cycle life (mA/cm^2)	Based on final $(Q_a - Q_c)$ at 1000 cycles (mA/cm^2)
1	Chill-cast pure Pb	0.163	0.154
5	Ternary wrought Pb/0.07 Ca/0.70 Sn	0.160	0.159
4	Pure wrought Pb	0.150	0.155
2	Chill-cast ternary Pb/0.54 Ca/0.70 Sn	0.143	0.146
3	Pb/5.7 Sn	0.115	0.116

TABLE 2

Weight gain during oxidation of Pb/0.054 Ca/0.70 Sn in cyclic voltammetry

	Experiment No.		
	1	2	3
Surface area (cm^2)	4.12	4.35	3.86
$Q_a - Q_c$ at end of 1000 cycles (C)	116.0	114.9	99.6
$Q_a - Q_c$ per unit area (C/cm^2)	28.2	26.4	25.8
Weight gain exp. (mg/cm^2)	3.2	3.0	4.1
Weight gain calculated from weight loss during stripping (mg/cm^2)	4.4	3.5	5.6
Calculated from net anodic charge $Q_a - Q_c$:			
4 electron transfer (mg/cm^2)	7.0	6.6	6.4
2 electron transfer (mg/cm^2)	14.0	13.2	12.8

respectively, for chill-cast ternary Pb/Ca/Sn alloy, wrought Pb/5.7 Sb, wrought ternary Pb/Ca/Sn alloy, chill-cast pure Pb, and wrought pure Pb. These values may have a large error because of the small absolute quantity of the weight change and because of some small losses due to shedding and washing off the electrodes. However, the weight changes still show internal consistency and corroborate the 4 electron transfer mechanism of the oxidation reaction. For example, data for three ternary Pb–Ca–Sn alloy electrodes are listed in Table 2. The weight gain can be ascribed to a stoichiometric change from Pb to $PbSO_4$ although 10 to 20% of the reaction product, represented by the net anodic charge $Q_a - Q_c$, was in the form of PbO_2.

Corresponding values are given for the weight gain calculated from the weight loss on stripping off the oxidation product at the end of the experiment.

Finally, the quantities $Q_a - Q_c$ are calculated in terms of weight gain corresponding to the accumulation of the experimentally determined

charge, based on a 4 electron transfer ($Pb \rightarrow PbO_2$) and on a 2 electron transfer ($Pb \rightarrow PbSO_4$).

Anodization at constant potential

A period of 24 hours was chosen arbitrarily as a convenient time for the constant potential tests. After the initial decay of the current, which occurs in the first few minutes due to the passivation by the oxidation product, PbO_2, the subsequent anodizing current increases linearly at first and then somewhat more rapidly during the course of the experiment. Two valid parameters for the evaluation of the oxidation process are: (i) the average current density over the total period of 24 hours, and (ii) the final current density after 24 h at constant potential. Both these quantities are shown in Tables 3 and 4 for the different grid materials at constant potential anodization of 1.300 and 1.400 V *vs.* Hg/Hg_2SO_4. They are arranged in the order of decreasing magnitude.

TABLE 3

Anodization at constant potential of 1.300 V *vs.* Hg/Hg_2SO_4

Material		Anodic current densities (mA/cm^2)	
		Average value over 24 h	Final value after 24 h
3	Cast Pb/5.7 Sb	0.0426	0.137
4	Wrought pure Pb	0.0460	0.0516
1	Chill-cast pure Pb	0.0187	0.0266
5	Wrought ternary alloy Pb/0.07 Ca/0.70 Sn	0.0103	0.0097
2	Chill-cast ternary alloy Pb/0.053 Ca/0.70 Sn	0.0063	0.0063

TABLE 4

Anodization at constant potential of 1.400 V *vs.* Hg/Hg_2SO_4

Material		Anodic current densities (mA/cm^2)	
		Average value after 24 h	Final value after 24 h
4	Wrought pure Pb	0.141	0.238
3	Cast Pb/5.7 Sb	0.107	0.170
2	Chill-cast ternary alloy Pb/0.053 Ca/0.70 Sn	0.0449	0.0497
5	Wrought ternary alloy Pb/0.07 Ca/0.70 Sn	0.0334	0.0465
1	Chill-cast pure Pb	0.0211	0.081

Discussion

In this work the extent to which cyclic voltammetry can simulate the cycling of a battery grid in actual service life was to be established. Others have shown [1 - 7] that cyclic voltammetry of the PbO_2 electrode is extremely sensitive to the pretreatment of the electrode. For example, Sharp [3] showed the influence of the anodic treatment on subsequent cathodic potential sweeps. In the present case simpler and reproducible voltammograms were obtained by choosing repetitive cycling in the potential range between the conditions of complete charge and discharge of the positive plate of the lead–acid cell. This simplified the electrochemistry occurring at the electrode. It produced approximately an anodic current density corresponding to that encountered in lead grid corrosion. Any appreciable simultaneous oxygen evolution was avoided by restricting the anodic peak potential to a region of high oxygen overvoltage and limiting the time during which the electrode was at that potential. Consequently, it was thought that the CV procedure should yield at least a qualitative ranking of Pb and Pb alloy corrosion resistance for grid materials.

The electrochemical reactions involve: (i) the oxidation (corrosion) of the substrate, *i.e.* a direct anodization of Pb to PbO_2 during the charging portion of the cycle. Pb may also be oxidized to a Pb(II) compound on current reversal, during the discharging portion of the cycle, which is still sufficiently anodic to produce PbO or the basic lead sulfates; while (ii) most of the oxidation product, PbO_2 is reduced to $PbSO_4$.

Formation of inactive PbO_2

The value of the cathodic charge, Q_c, clearly represents the reduction or discharge reaction. However, the net charge difference, $Q_a - Q_c$, may not necessarily be identified with (i) above, because (i) concerns the oxidation of the substrate, which cumulatively continues in each cycle and participates in the redox process, whereas $Q_a - Q_c$ is the 1 to 5% of oxidation product that is irreversibly oxidized. The accumulation of non-dischargeable reaction product corresponds to PbO_2, rendered inactive by structural changes during cycling which have been previously discussed in the literature [11, 12]. In battery terminology, the parameter $Q_a - Q_c$ is, therefore, related to the active plate material as well as the corrosion product of the grid. To a smaller extent $Q_a - Q_c$ contains also the charge used in producing oxygen, as discussed above.

The increase of the parameter $\Sigma(Q_a - Q_c)$ proceeded at a constant rate during the cycle life for all materials (Fig. 9). The average current density for the process leading to the inactivation of the oxidation product was calculated from the accumulated charge (Table 1). The Pb–5.7 Sb alloy had the smallest effect whereas the other four samples showed about the same increase of $Q_a - Q_c$ although that for the chill-cast ternary alloy was outside the experimental uncertainty of the range of the others and intermediate between antimonial and non-antimonial grids. Thus, a qualitative ranking in

the order of least to most formation of inactive material is:

$$\text{Pb/Sb} \ll \text{chill-cast ternary alloy} < \text{chill-cast pure Pb} = \text{wrought Pb} = \text{wrought ternary alloy}$$

This observation supports the view of Ritchie and Burbank [13] who attribute the beneficial effect of Sb in the positive plate to its function as a nucleating agent for PbO_2 which simultaneously inhibits crystal growth. Thus, the deleterious geometrical effects which lead to the formation of inactive PbO_2 are partly avoided.

As pointed out above, the extent to which $Q_a - Q_c$ may also be associated with an accumulation of corrosion product is less clear. However, the present results show that for the experimental conditions of these tests the studied samples have about the same anodic activity with the exception of the Pb/Sb alloy.

Cathodic charge (discharge of reaction product)

The distinction in the discharge behavior of the ternary Pb–Ca–Sn alloys as compared with the pure Pb and Pb–Sb alloy (Fig. 10) is remarkable. Whereas anodic activity continued at an approximately constant rate with cycle life for all samples, the cathodic charge Q_c reached a limiting value after 150 to 200 cycles for the ternary alloys. The value of Q_c continued to increase for the other materials. Furthermore, it should be noted that although the incremental values per cycle for $Q_a - Q_c$ were all about 0.025 C/cm^2; those of Q_c at the constant value for the ternary alloys were about 0.5 C/cm^2 but for the others Q_c increased to about 1.5 C/cm^2. The underlying mechanism for this observation is not clear. Some barrier mechanism must operate which limits the amount of reversibly formed anodic product to a constant value. Continuous [14] and discontinuous [9] barrier layers at the solid–solid Pb–PbO_2 interface have been previously observed. A diffusion-limited chemical species, either in the solid reaction product or in the electrolyte-depleted liquid solution, may be another possible source of the reaction limitation.

Weight changes

The weight gain due to corrosion or the weight loss on removal of the corrosion layer are quantitative measures of the corrosion reactions. In the present work these determinations correlate qualitatively with the quantity $Q_a - Q_c$. However, the total amount of the oxide and sulfate layer was too small for more than qualitative agreement with the electrochemical measurements. Table 2 shows the experimental weight gain of three samples in the amount of 3.2, 3.0 and 4.1 mg/cm^2. Tabulated also is the calculated weight gain based on the experimentally determined weight loss on stripping the corrosion layer, *viz.* 4.4, 3.5, and 5.6 mg/cm^2. This assumes that all of the oxidation product was $PbSO_4$. Some of it consisted of irreversibly oxidized PbO_2. Assuming this to be 20%, the calculated values based on stripping experiments would be 3.8, 3.0, and 4.9 mg/cm^2 in better agreement with the

experimental values. Finally, the weight changes calculated from $Q_a - Q_c$, *i.e.* 7.0, 6.6 and 6.4 mg/cm^2, indicate qualitative consistency. They also show that the process involves a 4-electron transfer (Pb → PbO_2). The irreversibly oxidized product is some form of PbO_2.

Anodization at constant potential

Tables 3 and 4 show current densities for potentials at 1.300 and 1.400 V, arranged in the order of decreasing anodic activity. The results must be viewed separately because at the higher potential there is considerable, and even a major, contribution to the current by the oxygen evolution reaction. The current density increased linearly over the total time of 24 hours only for the two ternary alloys at 1.300 V and for the chill-cast pure Pb and possibly for the chill-cast ternary alloy at 1.400 V. These materials may be considered to have had the least oxygen evolution.

Our previous work [5] was intended to evaluate corrosion behavior of various Pb samples for float application at a potential of 1.34 V *vs.* Hg/Hg_2SO_4 over a period of 7 months (about 5000 hours). Several different electrodes were tested in parallel in the same cell so that the corrosion current densities of 0.050 mA/cm^2 (flooded cell) and 0.043 mA/cm^2 (starved cell) represented average values. However, these values are consistent with and correlate well with the data of Tables 3 and 4.

Grain structure of lead and lead alloys

Consideration of the grain structure of a test sample is important for a corrosion study since the intergranular and intragranular mechanisms of corrosion largely determine the rates of the reactions. This has been shown particularly well for lead–calcium alloys by Rose and Young [15]. They showed the effect of grain size on the mode of corrosive attack, distinguishing between the higher penetration but lower weight loss found in large grained samples as compared with the small, grain-refined structure of wrought materials. In the present study, the two chill-cast samples had the typical large grain structure (Figs. 3, 4 and 5). The grain-refined structure of the ternary wrought alloy (Fig. 8) and the dendritic structure of the Pb/Sb alloy (Fig. 6) are also typical of previously observed samples. However, the wrought pure Pb was free of small grain sizes (Fig. 7). Furthermore, since its grain sizes are comparable to those of the chill-cast materials (both pure Pb and ternary alloy), it would have been expected that the wrought pure Pb should have similar anodic activity. But the corrosion rate at constant potential was considerably larger for this material, in spite of the large grain sizes.

Conclusions

In conclusion, cyclic voltammetry, electrochemical measurements at constant potential, and metallography were used to follow the anodic activity of various samples of Pb and Pb alloys.

Both the processing by chill-casting and the ternary composition had a beneficial effect on lowering the anodic activity which here can be identified with corrosion of the candidate grid alloys. This is illustrated by the comparative ranking of the materials in the order of least to most anodic activity at the two potentials:

At 1.300 V *vs.* Hg/Hg_2SO_4: chill-cast ternary alloy < wrought ternary alloy < chill-cast pure Pb < Pb/Sb = wrought pure Pb

At 1.400 V *vs.* Hg/Hg_2SO_4: chill-cast pure Pb < wrought ternary alloy = chill-cast ternary alloy < Pb/Sb < wrought pure Pb.

The constant potential measurements yielded results in line with the expectation that the large-grained chill-cast samples would have the least corrosion whereas the Pb/Sb alloy and wrought pure Pb had a greater average corrosion current density. The wrought Pb, although barely distinguishable in microstructure, behaved differently from the chill-cast pure Pb.

In cyclic voltammetry the samples were cycled over the potential range corresponding to that of the positive grid of the lead–acid battery. The results were more informative with respect to the reaction mechanisms than for predicting corrosion behavior, because all samples except the Pb/Sb alloy, exhibited about the same quantitative anodic activity. With regard to the mechanism of the electrode reactions, there was evidence that irreversible PbO_2 was formed. A diffusion or barrier-limited process was also brought to light during the cathodic discharge of calcium-containing ternary Pb–Ca–Sn alloys, in sharp distinction to the behavior of pure Pb and Pb/Sb samples.

Acknowledgements

The author thanks R. F. Thornton for valuable discussions during the course of this work. Thanks are also due to D. G. Fink, I. L. Mella and C. R. Rodd, members of the R & DC Metallography group, for their valuable contribution to this work.

This paper was originally presented at the 150th Fall Meeting of the Electrochemical Society, Inc., in Las Vegas, Nevada, U.S.A., October 1976.

References

1 H. S. Panesar, in D. H. Collins (ed.), Power Sources, Vol. 3, Oriel Press, Newcastle upon Tyne, 1971, p. 79.
2 J. P. Carr, N. A. Hampson and R. Taylor, J. Electroanal. Chem., 33 (1971) 109.
3 T. F. Sharpe, J. Electrochem. Soc., 122 (1975) 845.
4 T. G. Chang, M. M. Wright and E. M. Valeriote, in D. H. Collins (ed.), Power Sources, Vol. 6, Academic Press, London, to be published.

5 T. F. Sharpe, J. Electrochem. Soc., 124 (1977) 168.
6 E. M. L. Valeriote and L. D. Gallop, ibid., 124 (1977) 370.
7 K. R. Bullock and D. M. McClelland, Electrochem. Soc., Battery Div., Extended Abstr., Oct. 1976, p. 45.
8 P. Ruetschi, R. T. Angstadt and B. D. Cahan, J. Electrochem. Soc., 106 (1959) 547.
9 J. L. Weininger and E. G. Siwek, J. Electrochem. Soc., 123 (1976) 603.
10 T. W. Caldwell and U. S. Sokolov, J. Electrochem. Soc., 123 (1976) 972.
11 A. C. Simon, S. M. Caulder and J. T. Stemmle, J. Electrochem. Soc., 122 (1975) 461.
12 B. Burrows and H. Giess, J. Electrochem. Soc., 122 (1975) 1640.
13 E. J. Ritchie and J. Burbank, J. Electrochem. Soc., 117 (1970) 299.
14 S. Tudor, A. Weisstuch and S. H. Davang, Electrochem. Technol., 3 (1965) 90; 4 (1966) 406; and 5 (1967) 21.
15 M. V. Rose and J. A. Young, Proc. 5th Int. Lead Conf., Paris, Nov. 1974.